

Finite deformation elasto-plastic consolidation analysis of soft clay by the weak form quadrature element method

Shuai YUAN, Hong-zhi ZHONG^{†‡}

(Department of Civil Engineering, Tsinghua University, Beijing 100084, China)

[†]E-mail: hzz@tsinghua.edu.cn

Received Oct. 11, 2016; Revision accepted Feb. 10, 2017; Crosschecked Nov. 15, 2017

Abstract: A weak form quadrature element formulation is established for finite deformation consolidation problems of an elasto-plastic saturated soft clay. The total Lagrangian (TL) description scheme and the weak form description of Biot's theory are adopted in the derivation of the formulation. The constitutive model of the soil skeleton is based on a multiplicative decomposition of the deformation gradient into elastic and plastic parts. The exponential flow relation between the velocity of pore fluid and hydraulic gradient is used to describe the continuity condition in Biot's theory. Results of numerical examples are compared with those of ABAQUS and previous studies, and very good agreement is reached, demonstrating the reliability and efficiency of the present formulation. The effect of non-Darcian flow on consolidation in the finite strain range is discussed and it is shown that, with the increase of the non-Darcian model parameters, the rate of consolidation and the differential settlement decrease.

Key words: Weak form quadrature element method; Finite deformation elasto-plastic consolidation; Soft clay; Multiplicative decomposition; Non-Darcian flow; Biot's theory
<http://dx.doi.org/10.1631/jzus.A1600671>

CLC number: TU44


1 Introduction

The 3D consolidation theory has found widespread application since it was put forward by Biot (1941). The variational principle of Biot's theory was first established by Sandhu and Wilson (1969) who studied linear consolidation by the finite element method. Nonlinear consolidation analysis was initiated by Lewis *et al.* (1976) using the Duncan-Chang model. Since then various constitutive models of soils have been used in nonlinear consolidation analyses that are needed in many geotechnical engineering projects such as road embankments, building foundations, and tailings impoundments.

Large deformation is often observed when soft clay, which has high void ratio and volume com-

pressibility, is loaded. The conventional small deformation consolidation analysis is no longer sufficient and extension to a finite strain range to account for the effect of geometrical nonlinearity is needed. Substantial research has been done on large deformation consolidation theory. The 1D large deformation consolidation theory was put forward by Mikasa (1965) and Gibson *et al.* (1967). In their work, void ratio was chosen as a basic variable which means that their work cannot be extended to 3D cases. Carter *et al.* (1977; 1979) developed 3D finite elastic consolidation and finite elasto-plastic consolidation theories using a spatial description. An implicit-explicit scheme for finite strain consolidation analysis was proposed by Prévost (1983). Additive elasto-plastic decomposition was primarily used in the constitutive model of the soil skeleton in some earlier work. The shortcomings of additive decomposition were pointed out by Borja and Alarcón (1995) and Borja *et al.* (1998) who employed the multiplicative

[‡] Corresponding author

 ORCID: Shuai YUAN, <http://orcid.org/0000-0002-8288-6858>
© Zhejiang University and Springer-Verlag GmbH Germany 2017

decomposition of the deformation gradient for the solid phase. Armero (1999) used the Cauchy pore pressure and considered the additive elasto-plastic decomposition of the fluid content. Xie *et al.* (1994) proposed a 3D large deformation consolidation theory based on the respective spatial and material descriptions (Xie *et al.*, 1995) and derived the total Lagrangian (TL) formulation of the finite element method. The updated Lagrangian (UL) formulation based on the same 3D large deformation consolidation theory was derived by Li (2001) and the arbitrary Lagrangian Eulerian (ALE) formulation by Kuang (2010). Large strain consolidation of very soft clay was studied by Hu *et al.* (2013) using elastic viscoplastic constitutive models. In their work, the necessity of large strain compressibility and creep effects was verified. Kardani *et al.* (2014) implemented some higher order elements in the analysis of large strain consolidation problems and showed that the number of degrees of freedom and computer running time could therefore be significantly decreased.

Overall, the aforementioned research is mainly focused on constitutive models of the solid skeleton. Properties of the fluid phase have been seldom studied and Darcy's law has been assumed virtually unanimously. However, as shown by many researchers, the pore fluid flow may deviate from Darcy's law when the hydraulic gradient is low. An exponential law for the fluid flow in the whole range of hydraulic gradient was given by Slepicka (1960). Hansbo (1997; 2001) conducted a detailed study and found that an exponential relation between hydraulic gradient and velocity of pore fluid would reach a better agreement between theory and practice than linear Darcy's law when the hydraulic gradient is below a critical value. Non-Darcian laws have been broadly accepted, and models of consolidation based on non-Darcy flow soon emerged (Teh and Nie, 2002). However, these studies were mainly confined to 1D problems or cases under the condition of infinitesimal strain. To the best knowledge of the authors, multi-dimensional large deformation consolidation analysis with non-Darcian flow has been hardly ever seen. In the present work, finite deformation elasto-plastic consolidation of soft clay with non-Darcian flow is analyzed using the weak form quadrature element method (QEM). The QEM is an efficient numerical tool which has been successfully applied to various

structural problems (Mo *et al.*, 2009; Zhong and Gao, 2010; Zhong and Wang, 2010; He and Zhong, 2012) and has found some applications in geotechnical engineering (Yuan and Zhong, 2014; 2015). It should be mentioned that, pressure oscillations in consolidation analysis when small time increments are used (Preisig and Prévost, 2011; Wang *et al.*, 2013) will also be observed in the QEM. Some strategies have been proposed (Yuan, 2015) and the numerical instability has been greatly alleviated. In the QEM, integrals in the weak form description of a problem are first evaluated by numerical integration, and then the derivatives at an integration point are represented by the differential quadrature analogue. With the differential quadrature analogue, a derivative is approximated by the linear weighted sum of variables at sampling points. Thus, algebraic equations are established from which all the function variables are obtained. The QEM has the characteristics of global approximation and enjoys rapid convergence. In the following sections, a weak form description of large deformation consolidation theory is derived based on the initial configuration. Nodal displacements and the Cauchy pore pressure are used as the basic variables. A TL approach is employed wherein the Green strain and the second Piola-Kirchhoff stress are taken as the strain and stress variables, respectively. The exponential flow law developed by Hansbo (1997; 2001) is used for description of the continuity condition in Biot's theory. As to the solid phase, the finite-strain Cam-clay model in the framework of multiplicative decomposition put forward by Callari *et al.* (1998) is used. Results of numerical examples based on Darcy's law are compared with those from ABAQUS and other publications (Al-Tabbaa, 1987; Callari *et al.*, 1998; Borja *et al.*, 1998). The effect of geometric nonlinearity and non-Darcian flow relation on consolidation in finite strain range is discussed.

2 Formulation

In the present work, boldfaced letters indicate matrices and vectors; underlined boldfaced letters stand for their tensor form, and boldfaced letters with subscripts (i, j, k) designate their values at the node (i, j, k).

2.1 Non-Darcian flow

According to Hansbo (1997; 2001)’s work, the following flow law (Fig. 1) will give a more reasonable result:

$$\begin{cases} v_w^r = k_w i_w^m / (m i_1^{m-1}), & i_w \leq i_1, \\ v_w^r = k_w (i_w - (m-1)i_1/m), & i_w > i_1, \end{cases} \quad (1)$$

where v_w^r is the Darcian velocity of the pore fluid, k_w is the permeability coefficient, i_w is the hydraulic gradient, m is the exponent for hydraulic gradient, and i_1 is the interfacial hydraulic gradient for linear and exponential flow relations. It is seen from Eq. (1) that the exponential law holds when the hydraulic gradient is low. The linear relation is valid otherwise.

The relation between v_w^r , the vector of Darcian velocity of pore fluid, and ∇u_w , the spatial gradient of the Cauchy pore pressure u_w , can be obtained from Eq. (1) as

$$v_w^r = -K_w \nabla u_w, \quad (2)$$

with

$$K_w = \begin{bmatrix} a_1 & 0 & 0 \\ 0 & a_2 & 0 \\ 0 & 0 & a_3 \end{bmatrix}, \quad (3)$$

$$a_j = \begin{cases} k_{wj} \frac{1}{\mu_w^m} |u_{wj}|^{m-1} / (m i_1^{m-1}), & |u_{wj}| \leq \mu_w i_1, \\ \frac{k_{wj}}{\mu_w} \left(1 - \frac{m-1}{m} |u_{wj}| \mu_w i_1 \right), & |u_{wj}| > \mu_w i_1, \end{cases} \quad (4)$$

$j = 1, 2, 3,$

where K_w is the permeability matrix, μ_w is the dynamic viscosity of the pore fluid, and u_{wj} is the derivative of the pore pressure with respect to the j th coordinate. Isotropic permeability coefficients k_{wj} are assumed herein. Therefore, the permeability matrix remains unchanged during rotation. The permeability is assumed to vary with the void ratio e as

$$e - e_0 = c_k \lg(k_w / k_{w0}), \quad (5)$$

where c_k is the permeability index; e_0 and k_{w0} are the reference void ratio and reference permeability, respectively.

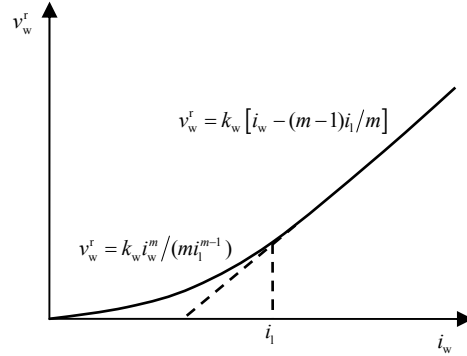


Fig. 1 Exponential flow law between the Darcian velocity of pore fluid and hydraulic gradient

2.2 Finite-strain Cam-clay model based on multiplicative decomposition

Consider the multiplicative decomposition of the deformation gradient \underline{F} :

$$\underline{F} = \underline{F}^e \underline{F}^p, \quad (6)$$

where \underline{F}^e and \underline{F}^p are the elastic and plastic parts of the deformation gradient, respectively. The elastic left Cauchy-Green strains $\underline{b}^e := \underline{F}^e \underline{F}^{eT}$ and the plastic right Cauchy-Green strains $\underline{C}^p := \underline{F}^{pT} \underline{F}^p$ are then interrelated by

$$\underline{b}^e = \underline{F}(\underline{C}^p)^{-1} \underline{F}^T. \quad (7)$$

According to the maximum dissipation principle, the evolutionary laws of the model read

$$\begin{aligned} \frac{1}{2} L_v \underline{b}^e &= \dot{\gamma} \left(\frac{\partial f(\underline{\tau}, \lambda)}{\partial \underline{\tau}} \right) \underline{b}^e, \\ \dot{\phi} &= -\dot{\gamma} \frac{\partial f(\underline{\tau}, \lambda)}{\partial \lambda}, \\ \dot{\gamma} &\geq 0, \quad f(\underline{\tau}, \lambda) \leq 0, \quad \dot{\gamma} f(\underline{\tau}, \lambda) = 0, \end{aligned} \quad (8)$$

where $L_v \underline{b}^e := \underline{F} \frac{\partial}{\partial t} (\underline{F}^{-1} \underline{b}^e \underline{F}^{-T}) \underline{F}^T$ is the Lie derivative of \underline{b}^e , $\dot{\gamma}$ is the time derivative of the plastic consistency parameter, $f(\underline{\tau}, \lambda)$ is the yield function, $\underline{\tau}$

is the Kirchhoff stress, λ is the stress-like hardening parameter, and $\dot{\varphi}$ is the time derivative of the strain-like hardening parameter. According to Simo (1992) and Simo and Meschke (1993), the expression of the yield function is the same as that in the scope of infinitesimal strain with the stress replaced by the Kirchhoff stress. The principle of objectivity restricts the yield function to be isotropic and by isotropy, and the principal directions of the Kirchhoff stress and those of the left elastic Cauchy-Green tensor coincide. Introduction of spectral decomposition into $\underline{\boldsymbol{\tau}}$ and $\underline{\boldsymbol{b}}^e$ gives

$$\underline{\boldsymbol{b}}^e = \sum_{j=1}^3 (\lambda_j^e)^2 \underline{\boldsymbol{n}}_j \otimes \underline{\boldsymbol{n}}_j, \quad (9)$$

$$\underline{\boldsymbol{\tau}} = \sum_{j=1}^3 \tau_j \underline{\boldsymbol{n}}_j \otimes \underline{\boldsymbol{n}}_j, \quad (10)$$

where $\underline{\boldsymbol{n}}_j$ are the principal directions of $\underline{\boldsymbol{b}}^e$ and $\underline{\boldsymbol{\tau}}$, λ_j^e are the principal stretches, and τ_j are the principal Kirchhoff stresses. Consider a time interval $[t_n, t_{n+1}]$ and follow the procedures of Simo (1992) and Simo and Meschke (1993), the return mapping algorithms are implemented in the principal axis defined by an elastic trial state $\underline{\boldsymbol{b}}^{e, n+1}$.

$$\begin{aligned} \varepsilon_j^{e, n+1} &= \varepsilon_j^{e, tr, n+1} + \Delta\gamma \frac{\partial f(\underline{\boldsymbol{\tau}}, \lambda)}{\partial \tau_j}, \quad j=1,2,3, \\ \varphi^{n+1} &= \varphi^n - \Delta\gamma \frac{\partial f(\underline{\boldsymbol{\tau}}, \lambda)}{\partial \lambda}, \\ \Delta\gamma &\geq 0, f(\underline{\boldsymbol{\tau}}, \lambda) \leq 0, \Delta\gamma f(\underline{\boldsymbol{\tau}}, \lambda) = 0, \end{aligned} \quad (11)$$

where $\varepsilon_j^e = -\ln(\lambda_j^e)$ are the principal logarithmic stretches, $\varepsilon_j^{e, tr, n+1}$ are the principal elastic trial logarithmic stretches, $\Delta\gamma$ is the increment of the plastic consistency parameter, and superscripts n and $n+1$ denote the values at time t_n and t_{n+1} , respectively. Define the unknown variable vector \boldsymbol{x} and the residual vector $\boldsymbol{y}(\boldsymbol{x})$, respectively, as

$$\boldsymbol{x} = \begin{bmatrix} \varepsilon_1^{e, n+1} \\ \varepsilon_2^{e, n+1} \\ \varepsilon_3^{e, n+1} \\ \Delta\gamma \end{bmatrix},$$

$$\boldsymbol{y}(\boldsymbol{x}) = \begin{bmatrix} \varepsilon_1^{e, n+1} - \varepsilon_1^{e, tr, n+1} - \Delta\gamma \frac{\partial f(\underline{\boldsymbol{\tau}}, \lambda)}{\partial \tau_1} \\ \varepsilon_2^{e, n+1} - \varepsilon_2^{e, tr, n+1} - \Delta\gamma \frac{\partial f(\underline{\boldsymbol{\tau}}, \lambda)}{\partial \tau_2} \\ \varepsilon_3^{e, n+1} - \varepsilon_3^{e, tr, n+1} - \Delta\gamma \frac{\partial f(\underline{\boldsymbol{\tau}}, \lambda)}{\partial \tau_3} \\ \varphi^{n+1} - \varphi^n + \Delta\gamma \frac{\partial f(\underline{\boldsymbol{\tau}}, \lambda)}{\partial \lambda} \end{bmatrix}. \quad (12)$$

A nonlinear equation $\boldsymbol{y}(\boldsymbol{x})=0$ is solved by the iterative procedure:

$$\delta \boldsymbol{x}^k = -(\boldsymbol{\Phi}^k)^{-1} \boldsymbol{y}^k, \quad \boldsymbol{\Phi} = \frac{\partial \boldsymbol{y}}{\partial \boldsymbol{x}}, \quad \boldsymbol{x}^{k+1} = \boldsymbol{x}^k + \delta \boldsymbol{x}^k, \quad (13)$$

where k is the number of iterations and $\boldsymbol{\Phi}$ is the gradient matrix. To overcome the shortcomings of the conventional linear $\check{v} - \ln \check{p}'$ law, bilogarithmic isotropic compression relations are adopted in the model (Fig. 2):

$$\ln \left(\frac{\check{v}}{\check{v}_p} \right) = -\check{k} \ln \left(\frac{\check{p}'}{\check{p}'_0} \right), \quad (14)$$

$$\ln \left(\frac{\check{v}_c}{\check{v}_{c0}} \right) = -\check{\lambda} \ln \left(\frac{\check{p}'_c}{\check{p}'_{c0}} \right), \quad (15)$$

where (\check{p}', \check{v}) , $(\check{p}'_c, \check{v}_c)$, and $(\check{p}'_{c0}, \check{v}_{c0})$ are the sets of the mean Kirchhoff effective stress and the specific volume pertaining to the current state, the initial yielding state, and the current yielding state, respectively; \check{v}_p is the specific volume by unloading the current state to the initial Kirchhoff pressure \check{p}'_0 ; $\check{\lambda}$ and \check{k} are the slopes for normal and over consolidation lines (Fig. 2), respectively.

The elastic strain energy function is given by

$$\check{W}(\underline{\boldsymbol{b}}^e) = \check{p}'_0 \check{k} \exp \left(\frac{\varepsilon_v^e}{\check{k}} \right) + \alpha \check{p}'_0 \exp \left(\frac{\varepsilon_v^e}{\check{k}} \right) \|\underline{\boldsymbol{e}}^e\|^2, \quad (16)$$

where $\varepsilon_v^e = -\ln(\lambda_1^e \lambda_2^e \lambda_3^e)$ is the elastic logarithmic volumetric strain, α is a model constant, and $\underline{\boldsymbol{e}}^e$ is the elastic principal logarithmic distortion defined by

$$\underline{\boldsymbol{e}}^e = [e_1^e \quad e_2^e \quad e_3^e]^T \quad \text{with} \quad e_i^e = -\frac{1}{3} \varepsilon_v^e - \ln(\lambda_i^e). \quad (17)$$

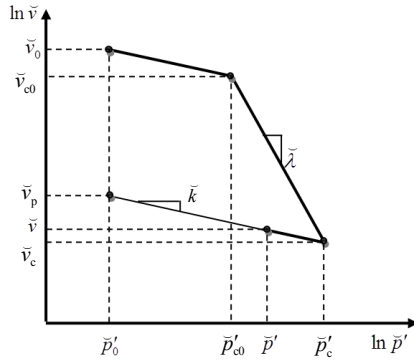


Fig. 2 Bilogarithmic isotropic compression relation

The yield criterion and hardening law are

$$f(\boldsymbol{\tau}, \bar{p}'_c) = \frac{\bar{q}^2}{M^2} + \bar{p}'(\bar{p}' - \bar{p}'_c) = 0, \tag{18}$$

$$\bar{p}'_c = \bar{p}'_{c0} \exp\left(\frac{\varepsilon_v^p}{\lambda - k}\right), \tag{19}$$

where $\varepsilon_v^p = -\ln J - \varepsilon_v^e$ is the plastic logarithmic volumetric strain, $J = \det(\mathbf{F})$ is the determinant of the deformation gradient, $\bar{q} := \sqrt{3/2} \|\text{dev}(\boldsymbol{\tau})\|$ is the deviatoric Kirchhoff stress, and M is the slope of the critical state line. \bar{p}'_c and ε_v^p are the stress-like and strain-like hardening parameters in the model, respectively.

The return mapping procedure in the space of the elastic principal logarithmic strains is employed here for stress integration. The material consistent tangent modulus \mathcal{C}^{ep} is obtained using the perturbation technique developed by Miehe (1996), which gives the relation between the second Piola-Kirchhoff stress \mathbf{S} and the Green strain \mathbf{E} :

$$d\mathbf{S} = \mathcal{C}^{ep} d\mathbf{E}. \tag{20}$$

2.3 Weak form description of large deformation consolidation

The equation of virtual work for the equilibrium condition in Biot's theory based on the initial configuration is

$$\int_{V_0} \delta \mathbf{E}^T \mathbf{S} dV_0 - \int_{V_0} \delta \mathbf{u}^T \mathbf{f}_0 dV_0 - \int_{A_0} \delta \mathbf{u}^T \mathbf{q}_0 dA_0 = 0, \tag{21}$$

where \mathbf{u} is the displacement, \mathbf{f}_0 is the body force per unit undeformed volume, \mathbf{q}_0 is the surface force per unit undeformed area, and A_0 and V_0 are the area and volume of the initial configuration, respectively. With the principle of effective stress, one has

$$\underline{\boldsymbol{\sigma}} = \underline{\boldsymbol{\sigma}}' + u_w \underline{\boldsymbol{\delta}}, \tag{22}$$

where $\underline{\boldsymbol{\sigma}}$ and $\underline{\boldsymbol{\sigma}}'$ are the total Cauchy stress and the effective Cauchy stress, respectively, and $\underline{\boldsymbol{\delta}}$ is the identity tensor. The transformation between the second Piola-Kirchhoff stress and the Cauchy stress is given by

$$\begin{aligned} \underline{\mathbf{S}} &= J \underline{\mathbf{F}}^{-1} \underline{\boldsymbol{\sigma}} \underline{\mathbf{F}}^{-T} \\ &= J \underline{\mathbf{F}}^{-1} \underline{\boldsymbol{\sigma}}' \underline{\mathbf{F}}^{-T} + J u_w \underline{\mathbf{F}}^{-1} \underline{\boldsymbol{\delta}} \underline{\mathbf{F}}^{-T} \\ &= \underline{\mathbf{S}}' + J u_w \underline{\mathbf{C}}^{-1}, \end{aligned} \tag{23}$$

where $\underline{\mathbf{C}}$ is the plastic right Cauchy-Green strain and $\underline{\mathbf{S}}'$ is the effective stress corresponding to the second Piola-Kirchhoff stress. Eq. (23) can be expressed in vectorial form as

$$\begin{aligned} \mathbf{S} &= \mathbf{S}' + \mathbf{M} u_w, \\ \mathbf{M} &= J \begin{bmatrix} \underline{\mathbf{C}}_{11}^{-1} & \underline{\mathbf{C}}_{22}^{-1} & \underline{\mathbf{C}}_{33}^{-1} & \underline{\mathbf{C}}_{23}^{-1} & \underline{\mathbf{C}}_{13}^{-1} & \underline{\mathbf{C}}_{12}^{-1} \end{bmatrix}^T. \end{aligned} \tag{24}$$

Introduction of Eq. (24) into Eq. (21) yields

$$\begin{aligned} \int_{V_0} \delta \mathbf{E}^T \mathbf{S}' dV_0 + \int_{V_0} \delta \mathbf{E}^T \mathbf{M} u_w dV_0 \\ - \int_{V_0} \delta \mathbf{u}^T \mathbf{f}_0 dV_0 - \int_{A_0} \delta \mathbf{u}^T \mathbf{q}_0 dA_0 = 0. \end{aligned} \tag{25}$$

Consider the following incremental expressions:

$$\begin{aligned} \mathbf{E}^{n+1} &= \mathbf{E}^n + \Delta \mathbf{E}, \quad \delta \mathbf{E}^{n+1} = \delta \Delta \mathbf{E}, \\ \mathbf{S}'^{n+1} &= \mathbf{S}'^n + \Delta \mathbf{S}', \quad \mathbf{u}^{n+1} = \mathbf{u}^n + \Delta \mathbf{u}, \\ \delta \mathbf{u}^{n+1} &= \delta \Delta \mathbf{u}, \quad u_w^{n+1} = u_w^n + \Delta u_w, \end{aligned} \tag{26}$$

where the superscripts n and $n+1$ indicate the values of the quantities at time instants t_n and t_{n+1} , respectively. Introduction of Eq. (26) into Eq. (25) at time t_{n+1} gives the following incremental weak form description of equilibrium:

$$\begin{aligned} & \int_{V_0} \delta \Delta \mathbf{E}^T \Delta \mathbf{S}' dV_0 + \int_{V_0} \delta \Delta \mathbf{E}^T (\mathbf{S}'^n + \mathbf{M}^{n+1} u_w^n) dV_0 \\ & + \int_{V_0} \delta \Delta \mathbf{E}^T \mathbf{M}^{n+1} \Delta u_w dV_0 \\ & = \int_{V_0} \delta \Delta \mathbf{u}^T \mathbf{f}_0^{n+1} dV_0 + \int_{A_0} \delta \Delta \mathbf{u}^T \mathbf{q}_0^{n+1} dA_0. \end{aligned} \quad (27)$$

The equation of continuity of porous fluid flow based on the current configuration is

$$\text{tr} \underline{\mathbf{l}} = \text{div} \underline{\mathbf{v}}_w^r, \quad (28)$$

where $\underline{\mathbf{l}}$ is the deformation rate tensor. Note that $\text{tr} \underline{\mathbf{l}} = \underline{\mathbf{C}}^{-1} : \underline{\dot{\mathbf{E}}}$ and Eq. (28) can be given in vectorial form as

$$\frac{\mathbf{M} \dot{\mathbf{E}}}{J} = \text{div} \underline{\mathbf{v}}_w^r, \quad (29)$$

where $\dot{\mathbf{E}}$ is the Green strain rate. The weak form description of continuity based on the current configuration is

$$\int_V \delta u_w \text{div} \underline{\mathbf{v}}_w^r dV - \int_V \delta u_w \frac{\mathbf{M} \dot{\mathbf{E}}}{J} dV = 0, \quad (30)$$

where V is the deformed volume. Integration of Eq. (30) by parts gives

$$\begin{aligned} & - \int_V (\nabla \delta u_w)^T \underline{\mathbf{v}}_w^r dV \\ & - \int_V \delta u_w \frac{\mathbf{M} \dot{\mathbf{E}}}{J} dV + \int_A \delta u_w v_n dA = 0, \end{aligned} \quad (31)$$

where A is the deformed area and v_n is the given normal velocity on boundary surfaces. Introduction of Eq. (2) into Eq. (31) yields

$$\begin{aligned} & \int_V (\nabla \delta u_w)^T \mathbf{K}_w \nabla u_w dV \\ & - \int_V \delta u_w \frac{\mathbf{M} \dot{\mathbf{E}}}{J} dV + \int_A \delta u_w v_n dA = 0. \end{aligned} \quad (32)$$

The following transformations are introduced:

$$\begin{aligned} \nabla u_w &= \mathbf{F}^{-T} \nabla_0 u_w, \quad dV = J dV_0, \\ dA &= J \mathbf{F}^{-T} dA_0, \quad \underline{\mathbf{v}}_w^r = J \mathbf{F}^{-1} \underline{\mathbf{v}}_w^r, \\ \mathbf{K}_{w0} &= J \mathbf{F}^{-1} \mathbf{K}_w \mathbf{F}^{-T}, \end{aligned} \quad (33)$$

where A and A_0 are the deformed area and undeformed area vectors, respectively; ∇_0 denotes the gradient with respect to the material configuration; $\underline{\mathbf{v}}_w^r$ and \mathbf{K}_{w0} are the Darcian velocity of the pore fluid and the permeability matrix based on the initial configuration, respectively. Then the weak form description of continuity based on the initial configuration is obtained as

$$\begin{aligned} & \int_{V_0} \delta u_w \mathbf{M}^T \dot{\mathbf{E}} dV_0 - \int_{A_0} \delta u_w v_n dA_0 \\ & - \int_{V_0} (\nabla_0 \delta u_w)^T \mathbf{K}_{w0} \nabla_0 u_w dV_0 = 0, \end{aligned} \quad (34)$$

where v_n denotes the normal velocity based on the initial configuration. Eqs. (27) and (34) are the weak form description of large deformation consolidation problems.

2.4 Weak form quadrature element formulation

In the QEM, the solution domain is usually first discretized into a few quadrilateral/hexahedral subdomains (elements) where numerical integration can be carried out. Then every subdomain is transformed onto the standard computational domain. In the case of a hexahedral subdomain, for instance, one has

$$\begin{aligned} X_j &= X_j(\xi_1, \xi_2, \xi_3), \\ -1 &\leq \xi_1, \xi_2, \xi_3 \leq 1, \quad j=1, 2, 3, \end{aligned} \quad (35)$$

where X_j are the coordinates in the undeformed physical domain; ξ_1, ξ_2, ξ_3 are the coordinates in the standard domain. With the chain rule of differentiation:

$$\begin{Bmatrix} \frac{\partial}{\partial \xi_1} \\ \frac{\partial}{\partial \xi_2} \\ \frac{\partial}{\partial \xi_3} \end{Bmatrix} = \mathbf{J} \begin{Bmatrix} \frac{\partial}{\partial X_1} \\ \frac{\partial}{\partial X_2} \\ \frac{\partial}{\partial X_3} \end{Bmatrix}, \quad (36)$$

$$\begin{Bmatrix} \frac{\partial}{\partial X_1} \\ \frac{\partial}{\partial X_2} \\ \frac{\partial}{\partial X_3} \end{Bmatrix} = \mathbf{J}^{-1} \begin{Bmatrix} \frac{\partial}{\partial \xi_1} \\ \frac{\partial}{\partial \xi_2} \\ \frac{\partial}{\partial \xi_3} \end{Bmatrix}, \quad (37)$$

where \mathbf{J} is the Jacobian matrix for coordinate transformation. Introduction of numerical integration into Eq. (27) yields

$$\begin{aligned} & \sum_{j=1}^{N_{\xi_1}} \sum_{w=1}^{N_{\xi_2}} \sum_{l=1}^{N_{\xi_3}} W_j W_w W_l \delta \Delta \mathbf{E}_{jwl}^T \Delta \mathbf{S}'_{jwl} |\mathbf{J}|_{jwl} \\ & + \sum_{j=1}^{N_{\xi_1}} \sum_{w=1}^{N_{\xi_2}} \sum_{l=1}^{N_{\xi_3}} W_j W_w W_l \delta \Delta \mathbf{E}_{jwl}^T \mathbf{M}_{jwl}^{n+1} (\Delta u_w)_{jwl} |\mathbf{J}|_{jwl} \\ & = \sum_{j=1}^{N_{\xi_1}} \sum_{w=1}^{N_{j_1}} \sum_{l=1}^{N_{j_2}} W_w W_l \delta \Delta \mathbf{u}_{wl}^T \mathbf{q}_{0jwl}^{n+1} |\bar{\mathbf{J}}| \\ & + \sum_{j=1}^{N_{\xi_1}} \sum_{w=1}^{N_{\xi_2}} \sum_{l=1}^{N_{\xi_3}} W_j W_w W_l \delta \Delta \mathbf{u}_{jwl}^T \mathbf{f}_{jwl}^{n+1} |\mathbf{J}|_{jwl} \\ & - \sum_{j=1}^{N_{\xi_1}} \sum_{w=1}^{N_{\xi_2}} \sum_{l=1}^{N_{\xi_3}} W_j W_w W_l \delta \Delta \mathbf{E}_{jwl}^T (\mathbf{S}'_{jwl} + \mathbf{M}_{jwl}^{n+1} (u_w)_{jwl}^n) |\mathbf{J}|_{jwl}, \end{aligned} \tag{38}$$

where W_j, W_w, W_l are the weighting coefficients of the integration scheme; N_{ξ_i} are the number of integration points, $i=1, 2, 3$; N_S is the numbers of surfaces where external surface loads are applied and N_{j_1}, N_{j_2} are the numbers of integration points in the j th surface; $|\mathbf{J}|$ and $|\bar{\mathbf{J}}|$ are the Jacobians for the element domain and its boundary. In the QEM, boundary points have to be adopted as the integration points to conveniently apply the boundary conditions and to compute the derivatives by the differential quadrature analogue. Therefore, the Lobatto quadrature is chosen. The components of the Green strain tensor are

$$E_{jl}^n = -\frac{1}{2} \left(\frac{\partial u_j^n}{\partial X_l} + \frac{\partial u_l^n}{\partial X_j} + \frac{\partial u_o^n}{\partial X_l} \frac{\partial u_o^n}{\partial X_j} \right), \tag{39}$$

$j, l, o = 1, 2, 3,$

and their incremental forms are

$$\begin{aligned} \Delta E_{jl} & = -\frac{1}{2} \left(\frac{\partial \Delta u_j}{\partial X_l} + \frac{\partial \Delta u_l}{\partial X_j} + \frac{\partial \Delta u_o}{\partial X_l} \frac{\partial \Delta u_o}{\partial X_j} \right. \\ & \quad \left. + \frac{\partial \Delta u_o}{\partial X_l} \frac{\partial u_o^n}{\partial X_j} + \frac{\partial u_o^n}{\partial X_l} \frac{\partial \Delta u_o}{\partial X_j} \right) \\ & = \Delta E_{jl}^{L_1} + \Delta E_{jl}^{L_2} + \Delta E_{jl}^{NL}, \end{aligned}$$

$$\begin{aligned} \Delta E_{jl}^{L_1} & = -\frac{1}{2} \left(\frac{\partial \Delta u_j}{\partial X_l} + \frac{\partial \Delta u_l}{\partial X_j} \right), \\ \Delta E_{jl}^{L_2} & = -\frac{1}{2} \left(\frac{\partial \Delta u_o}{\partial X_l} \frac{\partial u_o^n}{\partial X_j} + \frac{\partial u_o^n}{\partial X_l} \frac{\partial \Delta u_o}{\partial X_j} \right), \\ \Delta E_{jl}^{NL} & = -\frac{1}{2} \frac{\partial \Delta u_o}{\partial X_l} \frac{\partial \Delta u_o}{\partial X_j}, \end{aligned} \tag{40}$$

where u_j^n is the displacement in the j th direction.

$\Delta E_{jl}^{L_1}$ and $\Delta E_{jl}^{L_2}$, the first two parts of the incremental Green strain, vary linearly with $\Delta \mathbf{u}$; ΔE_{jl}^{NL} , the last term in Eq. (40), is the nonlinear part. The vector of the incremental Green strain is defined as

$$\begin{aligned} \Delta \mathbf{E} & = \\ & \left[\Delta E_{11} \quad \Delta E_{22} \quad \Delta E_{33} \quad 2\Delta E_{23} \quad 2\Delta E_{13} \quad 2\Delta E_{12} \right]^T \\ & = \Delta \mathbf{E}^{L_1} + \Delta \mathbf{E}^{L_2} + \Delta \mathbf{E}^{NL}. \end{aligned} \tag{41}$$

In the present work, derivatives at an integration point are approximated using the differential quadrature analogue. The essence of the differential quadrature analogue is the expression of a function derivative in terms of weighted linear summation of function values at all grid points. By the differential quadrature analogue, the first part of the incremental Green strain at a given integration point can be expressed in terms of nodal displacement vector $\Delta \mathbf{d}^e$ as

$$\begin{aligned} \Delta E_{jwl}^{L_1} & = - \left[\frac{\partial \Delta u_1}{\partial X_1} \quad \frac{\partial \Delta u_2}{\partial X_2} \quad \frac{\partial \Delta u_3}{\partial X_3} \quad \frac{\partial \Delta u_2}{\partial X_3} + \frac{\partial \Delta u_3}{\partial X_2} \right. \\ & \quad \left. \frac{\partial \Delta u_1}{\partial X_3} + \frac{\partial \Delta u_3}{\partial X_1} \quad \frac{\partial \Delta u_1}{\partial X_2} + \frac{\partial \Delta u_2}{\partial X_1} \right]_{jwl}^T \\ & = -\mathbf{D}_{jwl} \left[\frac{\partial \Delta u_1}{\partial \xi_1} \quad \frac{\partial \Delta u_1}{\partial \xi_2} \quad \frac{\partial \Delta u_1}{\partial \xi_3} \quad \frac{\partial \Delta u_2}{\partial \xi_1} \right. \\ & \quad \left. \frac{\partial \Delta u_2}{\partial \xi_2} \quad \frac{\partial \Delta u_2}{\partial \xi_3} \quad \frac{\partial \Delta u_3}{\partial \xi_1} \quad \frac{\partial \Delta u_3}{\partial \xi_2} \quad \frac{\partial \Delta u_3}{\partial \xi_3} \right]_{jwl}^T \\ & = -\mathbf{D}_{jwl} \left[C_{jo}^1 \Delta u_{1owl} \quad C_{wo}^2 \Delta u_{1jol} \quad C_{lo}^3 \Delta u_{1jwo} \right. \\ & \quad C_{jo}^1 \Delta u_{2owl} \quad C_{wo}^2 \Delta u_{2jol} \quad C_{lo}^3 \Delta u_{2jwo} \quad C_{jo}^1 \Delta u_{3owl} \\ & \quad \left. C_{wo}^2 \Delta u_{3jol} \quad C_{lo}^3 \Delta u_{3jwo} \right]^T \\ & = -\mathbf{D}_{jwl} \bar{\mathbf{B}}_{jwl} \Delta \mathbf{d}^e, \end{aligned} \tag{42}$$

where $\bar{\mathbf{B}}_{jwl}$ is the nominal strain matrix. C_{ol}^i are the weighting coefficients in the i th direction for first-order derivatives in the differential quadrature analogue which can be calculated as

$$C_{ol}^i = \frac{\prod_{j=1, j \neq o}^{N_{\xi_i}} (\xi_{io} - \xi_{ij})}{(\xi_{io} - \xi_{il}) \prod_{j=1, j \neq l}^{N_{\xi_i}} (\xi_{il} - \xi_{ij})}, \quad (43)$$

$$C_{oo}^i = - \sum_{j=1, j \neq o}^{N_{\xi_i}} C_{oj}^i, \quad o, l = 1, 2, \dots, N_{\xi_i} \text{ and } o \neq l,$$

where ξ_{ij} is the normalized coordinate of the integration point. Eq. (43) is deduced based on the polynomial basis functions. \mathbf{D}_{jwl} is the transformation matrix defined as

$$\mathbf{D}_{jwl} = \begin{bmatrix} I_{11} & I_{12} & I_{13} & 0 & 0 & 0 & 0 & 0 & 0 \\ 0 & 0 & 0 & I_{21} & I_{22} & I_{23} & 0 & 0 & 0 \\ 0 & 0 & 0 & 0 & 0 & 0 & I_{31} & I_{32} & I_{33} \\ 0 & 0 & 0 & I_{31} & I_{32} & I_{33} & I_{21} & I_{22} & I_{23} \\ I_{31} & I_{32} & I_{33} & 0 & 0 & 0 & I_{11} & I_{12} & I_{13} \\ I_{21} & I_{22} & I_{23} & I_{11} & I_{12} & I_{13} & 0 & 0 & 0 \end{bmatrix}, \quad (44)$$

$$\mathbf{I} = \mathbf{J}^{-1}.$$

For the second part of the incremental Green strain

$$\Delta \mathbf{E}_{jwl}^{L_2} = - \left[\begin{array}{ccc} \frac{\partial \Delta u_o}{\partial X_1} \frac{\partial u_o^n}{\partial X_1} & \frac{\partial \Delta u_o}{\partial X_2} \frac{\partial u_o^n}{\partial X_2} & \frac{\partial \Delta u_o}{\partial X_3} \frac{\partial u_o^n}{\partial X_3} \\ \frac{\partial \Delta u_o}{\partial X_2} \frac{\partial u_o^n}{\partial X_3} + \frac{\partial u_o^n}{\partial X_2} \frac{\partial \Delta u_o}{\partial X_3} & \frac{\partial \Delta u_o}{\partial X_1} \frac{\partial u_o^n}{\partial X_3} + \frac{\partial u_o^n}{\partial X_1} \frac{\partial \Delta u_o}{\partial X_3} & \\ \frac{\partial \Delta u_o}{\partial X_1} \frac{\partial u_o^n}{\partial X_2} + \frac{\partial u_o^n}{\partial X_1} \frac{\partial \Delta u_o}{\partial X_2} \end{array} \right]^T$$

$$= - \mathbf{A}_{jwl}^n \hat{\mathbf{J}}_{jwl} \left[\begin{array}{cccc} \frac{\partial \Delta u_1}{\partial \xi_1} & \frac{\partial \Delta u_1}{\partial \xi_2} & \frac{\partial \Delta u_1}{\partial \xi_3} & \frac{\partial \Delta u_2}{\partial \xi_1} \\ \frac{\partial \Delta u_2}{\partial \xi_2} & \frac{\partial \Delta u_2}{\partial \xi_3} & \frac{\partial \Delta u_3}{\partial \xi_1} & \frac{\partial \Delta u_3}{\partial \xi_2} & \frac{\partial \Delta u_3}{\partial \xi_3} \end{array} \right]^T$$

$$= - \mathbf{A}_{jwl}^n \hat{\mathbf{J}}_{jwl} \bar{\mathbf{B}}_{jwl} \Delta \mathbf{d}^e, \quad (45)$$

where \mathbf{A}_{jwl}^n , the gradient matrix, is defined as

$$\mathbf{A}_{jwl}^n = \begin{bmatrix} \frac{\partial u_1^n}{\partial X_1} & 0 & 0 & \frac{\partial u_2^n}{\partial X_1} & 0 & 0 & \frac{\partial u_3^n}{\partial X_1} & 0 & 0 \\ 0 & \frac{\partial u_1^n}{\partial X_2} & 0 & 0 & \frac{\partial u_2^n}{\partial X_2} & 0 & 0 & \frac{\partial u_3^n}{\partial X_2} & 0 \\ 0 & 0 & \frac{\partial u_1^n}{\partial X_3} & 0 & 0 & \frac{\partial u_2^n}{\partial X_3} & 0 & 0 & \frac{\partial u_3^n}{\partial X_3} \\ 0 & \frac{\partial u_1^n}{\partial X_3} & \frac{\partial u_1^n}{\partial X_2} & 0 & \frac{\partial u_2^n}{\partial X_3} & \frac{\partial u_2^n}{\partial X_2} & 0 & \frac{\partial u_3^n}{\partial X_3} & \frac{\partial u_3^n}{\partial X_2} \\ \frac{\partial u_1^n}{\partial X_3} & 0 & \frac{\partial u_1^n}{\partial X_1} & \frac{\partial u_2^n}{\partial X_3} & 0 & \frac{\partial u_2^n}{\partial X_1} & \frac{\partial u_3^n}{\partial X_3} & 0 & \frac{\partial u_3^n}{\partial X_1} \\ \frac{\partial u_1^n}{\partial X_2} & \frac{\partial u_1^n}{\partial X_1} & 0 & \frac{\partial u_2^n}{\partial X_2} & \frac{\partial u_2^n}{\partial X_1} & 0 & \frac{\partial u_3^n}{\partial X_2} & \frac{\partial u_3^n}{\partial X_1} & 0 \end{bmatrix}_{jwl}, \quad (46)$$

$\hat{\mathbf{J}}_{jwl}$, the auxiliary transformation matrix, is given by

$$\hat{\mathbf{J}}_{jwl} = \begin{bmatrix} \mathbf{J}^{-1} & 0 & 0 \\ 0 & \mathbf{J}^{-1} & 0 \\ 0 & 0 & \mathbf{J}^{-1} \end{bmatrix}_{jwl}. \quad (47)$$

For the nonlinear part of the incremental Green strain:

$$\Delta \mathbf{E}_{jwl}^{NL} = - \left[\begin{array}{ccc} \frac{1}{2} \frac{\partial \Delta u_o}{\partial X_1} \frac{\partial \Delta u_o}{\partial X_1} & \frac{1}{2} \frac{\partial \Delta u_o}{\partial X_2} \frac{\partial \Delta u_o}{\partial X_2} & \frac{1}{2} \frac{\partial \Delta u_o}{\partial X_3} \frac{\partial \Delta u_o}{\partial X_3} \\ \frac{\partial \Delta u_o}{\partial X_2} \frac{\partial \Delta u_o}{\partial X_3} & \frac{\partial \Delta u_o}{\partial X_1} \frac{\partial \Delta u_o}{\partial X_3} & \frac{\partial \Delta u_o}{\partial X_1} \frac{\partial \Delta u_o}{\partial X_2} \end{array} \right]^T_{jwl}$$

$$= - \frac{1}{2} \Delta \mathbf{A}_{jwl} \hat{\mathbf{J}}_{jwl} \bar{\mathbf{B}}_{jwl} \Delta \mathbf{d}^e, \quad (48)$$

where $\Delta \mathbf{A}_{jwl}$ is the incremental gradient matrix given by

$$\Delta \mathbf{A}_{jwl} = \begin{bmatrix} \frac{\partial \Delta u_1}{\partial X_1} & 0 & 0 & \frac{\partial \Delta u_2}{\partial X_1} & 0 & 0 & \frac{\partial \Delta u_3}{\partial X_1} & 0 & 0 \\ 0 & \frac{\partial \Delta u_1}{\partial X_2} & 0 & 0 & \frac{\partial \Delta u_2}{\partial X_2} & 0 & 0 & \frac{\partial \Delta u_3}{\partial X_2} & 0 \\ 0 & 0 & \frac{\partial \Delta u_1}{\partial X_3} & 0 & 0 & \frac{\partial \Delta u_2}{\partial X_3} & 0 & 0 & \frac{\partial \Delta u_3}{\partial X_3} \\ 0 & \frac{\partial \Delta u_1}{\partial X_3} & \frac{\partial \Delta u_1}{\partial X_2} & 0 & \frac{\partial \Delta u_2}{\partial X_3} & \frac{\partial \Delta u_2}{\partial X_2} & 0 & \frac{\partial \Delta u_3}{\partial X_3} & \frac{\partial \Delta u_3}{\partial X_2} \\ \frac{\partial \Delta u_1}{\partial X_3} & 0 & \frac{\partial \Delta u_1}{\partial X_1} & \frac{\partial \Delta u_2}{\partial X_3} & 0 & \frac{\partial \Delta u_2}{\partial X_1} & \frac{\partial \Delta u_3}{\partial X_3} & 0 & \frac{\partial \Delta u_3}{\partial X_1} \\ \frac{\partial \Delta u_1}{\partial X_2} & \frac{\partial \Delta u_1}{\partial X_1} & 0 & \frac{\partial \Delta u_2}{\partial X_2} & \frac{\partial \Delta u_2}{\partial X_1} & 0 & \frac{\partial \Delta u_3}{\partial X_2} & \frac{\partial \Delta u_3}{\partial X_1} & 0 \end{bmatrix}_{jwl}. \quad (49)$$

Combination of Eqs. (42), (45), and (48) turns the incremental Green strain into

$$\begin{aligned} \Delta \mathbf{E}_{jwl} &= - \left(\mathbf{D}_{jwl} + \mathbf{A}_{jwl}^n \hat{\mathbf{J}}_{jwl} + \frac{1}{2} \Delta \mathbf{A}_{jwl} \hat{\mathbf{J}}_{jwl} \right) \bar{\mathbf{B}}_{jwl} \Delta \mathbf{d}^e \quad (50) \\ &= \mathbf{B}_{jwl}^1 \Delta \mathbf{d}^e, \end{aligned}$$

where \mathbf{B}_{jwl}^1 is the first strain matrix. It can be proved that:

$$\begin{aligned} &\delta(\Delta \mathbf{A}_{jwl} \hat{\mathbf{J}}_{jwl} \bar{\mathbf{B}}_{jwl} \Delta \mathbf{d}^e) \\ &= \delta \Delta \mathbf{A}_{jwl} \hat{\mathbf{J}}_{jwl} \bar{\mathbf{B}}_{jwl} \Delta \mathbf{d}^e + \Delta \mathbf{A}_{jwl} \delta \hat{\mathbf{J}}_{jwl} \bar{\mathbf{B}}_{jwl} \Delta \mathbf{d}^e \quad (51) \\ &= 2 \Delta \mathbf{A}_{jwl} \hat{\mathbf{J}}_{jwl} \bar{\mathbf{B}}_{jwl} \delta \Delta \mathbf{d}^e. \end{aligned}$$

Thus, the variation of the incremental Green strain is

$$\begin{aligned} \delta \Delta \mathbf{E}_{jwl} &= -(\mathbf{D}_{jwl} + \mathbf{A}_{jwl}^n \hat{\mathbf{J}}_{jwl} + \Delta \mathbf{A}_{jwl} \hat{\mathbf{J}}_{jwl}) \bar{\mathbf{B}}_{jwl} \delta \Delta \mathbf{d}^e \quad (52) \\ &= \mathbf{B}_{jwl}^2 \delta \Delta \mathbf{d}^e, \end{aligned}$$

where \mathbf{B}_{jwl}^2 is the second strain matrix. Introduction of Eqs. (20), (50), and (52) into Eq. (38) yields

$$(\mathbf{K}_s^e - \mathbf{K}_D^e) \Delta \mathbf{d}^e + \mathbf{K}_c^e \Delta \mathbf{u}_w^e = \mathbf{R}_F^e, \quad (53)$$

where \mathbf{u}_w^e is the element pore pressure vector. The stiffness matrix of the soil skeleton \mathbf{K}_s^e , the initial stress matrix \mathbf{K}_D^e , the coupling coefficient matrix \mathbf{K}_c^e , and the element load vector \mathbf{R}_F^e are given by

$$\begin{aligned} \mathbf{K}_s^e &= \sum_{j=1}^{N_{s1}} \sum_{w=1}^{N_{s2}} \sum_{l=1}^{N_{s3}} W_j W_w W_l |\mathbf{J}|_{jwl} \mathbf{B}_{jwl}^{2T} \mathbf{C}^{ep} \mathbf{B}_{jwl}^1, \\ \mathbf{K}_c^e &= \sum_{j=1}^{N_{s1}} \sum_{w=1}^{N_{s2}} \sum_{l=1}^{N_{s3}} W_j W_w W_l |\mathbf{J}|_{jwl} \mathbf{B}_{jwl}^{2T} \mathbf{M}_{jwl}^{n+1} \mathbf{G}_{jwl}, \\ \mathbf{K}_D^e &= \sum_{j=1}^{N_{s1}} \sum_{w=1}^{N_{s2}} \sum_{l=1}^{N_{s3}} (W_j W_w W_l |\mathbf{J}|_{jwl} \\ &\quad \cdot \bar{\mathbf{B}}_{jwl}^T \hat{\mathbf{J}}_{jwl}^T \mathbf{V}_{jwl}^n \hat{\mathbf{J}}_{jwl} \bar{\mathbf{B}}_{jwl}), \end{aligned}$$

$$\begin{aligned} \mathbf{R}_F^e &= \sum_{j=1}^{N_s} \sum_{w=1}^{N_{j1}} \sum_{l=1}^{N_{j2}} W_w W_l |\bar{\mathbf{J}}|_{w|} \mathbf{D}_{wl}^q \mathbf{q}_{0w}^{n+1} \\ &\quad + \sum_{j=1}^{N_{s1}} \sum_{w=1}^{N_{s2}} \sum_{l=1}^{N_{s3}} W_j W_w W_l |\mathbf{J}|_{jwl} \mathbf{D}_{jwl}^f \mathbf{f}_{0jwl}^{n+1} \\ &\quad + \sum_{j=1}^{N_{s1}} \sum_{w=1}^{N_{s2}} \sum_{l=1}^{N_{s3}} [W_j W_w W_l |\mathbf{J}|_{jwl} \bar{\mathbf{B}}_{jwl}^T \\ &\quad \cdot (\mathbf{D}_{jwl} + \mathbf{A}_{jwl}^n \hat{\mathbf{J}}_{jwl})^T (\mathbf{S}_{jwl}' + \mathbf{M}_{jwl}^{n+1} (\mathbf{u}_w)_{jwl}^n)], \quad (54) \end{aligned}$$

where \mathbf{G}_{jwl} is the connectivity vector for nodal pore pressure and the element pore pressure vector, $(\Delta \mathbf{u}_w)_{jwl} = \mathbf{G}_{jwl} \Delta \mathbf{u}_w^e$; \mathbf{D}_{wl}^q is the connectivity matrix for the boundary nodal displacements and the element displacement vector, $\delta \Delta \mathbf{u}_w^T = \delta \Delta \mathbf{d}^{eT} \mathbf{D}_{wl}^q$; \mathbf{D}_{jwl}^f is the connectivity matrix for the nodal displacements and the element displacement vector, $\delta \Delta \mathbf{u}_w^T = \delta \Delta \mathbf{d}^{eT} \mathbf{D}_{jwl}^f$. \mathbf{V}_{jwl}^n , the matrix concerning the initial stress, is given by

$$\begin{aligned} \mathbf{V}_{jwl}^n &= \begin{bmatrix} \boldsymbol{\eta}_{jwl}^n & 0 & 0 \\ 0 & \boldsymbol{\eta}_{jwl}^n & 0 \\ 0 & 0 & \boldsymbol{\eta}_{jwl}^n \end{bmatrix}, \\ \boldsymbol{\eta}_{jwl}^n &= \begin{bmatrix} S_1'^n + M_1^{n+1} u_w^n & S_6'^n + M_6^{n+1} u_w^n & S_5'^n + M_5^{n+1} u_w^n \\ S_6'^n + M_6^{n+1} u_w^n & S_2'^n + M_2^{n+1} u_w^n & S_4'^n + M_4^{n+1} u_w^n \\ S_5'^n + M_5^{n+1} u_w^n & S_4'^n + M_4^{n+1} u_w^n & S_3'^n + M_3^{n+1} u_w^n \end{bmatrix}_{jwl}. \quad (55) \end{aligned}$$

In a similar way, the integrals in the continuity condition are numerically evaluated by

$$\begin{aligned} &\frac{1}{\Delta t} \sum_{j=1}^{N_{s1}} \sum_{w=1}^{N_{s2}} \sum_{l=1}^{N_{s3}} W_j W_w W_l |\mathbf{J}|_{jwl} (\delta \mathbf{u}_w)_{jwl} \mathbf{M}_{jwl}^{n+1T} \Delta \mathbf{E}_{jwl} \\ &\quad - \sum_{j=1}^{N_v} \sum_{w=1}^{N_{j1}} \sum_{l=1}^{N_{j2}} W_w W_l |\bar{\mathbf{J}}|_{w|} (\delta \mathbf{u}_w)_{w|} (\mathbf{V}_n)_{w|} \\ &\quad - \sum_{j=1}^{N_{s1}} \sum_{w=1}^{N_{s2}} \sum_{l=1}^{N_{s3}} W_j W_w W_l |\mathbf{J}|_{jwl} (\nabla_0 \delta \mathbf{u}_w)_{jwl}^T (\mathbf{K}_{w0})_{jwl} (\nabla_0 \mathbf{u}_w)_{jwl} \\ &= 0, \quad (56) \end{aligned}$$

where $\dot{\mathbf{E}}$ is replaced by $\Delta \mathbf{E} / \Delta t$ and N_v is the number

of surfaces with given normal Darcian velocity. With the differential quadrature analogue, the material gradient of the Cauchy pore pressure at point (j, w, l) is given as

$$\begin{aligned}
 (\nabla_0 \mathbf{u}_w)_{jwl} &= \begin{Bmatrix} \frac{\partial u_w}{\partial X_1} \\ \frac{\partial u_w}{\partial X_2} \\ \frac{\partial u_w}{\partial X_3} \end{Bmatrix}_{jwl} = \mathbf{J}_{jwl}^{-1} \begin{Bmatrix} \frac{\partial u_w}{\partial \xi_1} \\ \frac{\partial u_w}{\partial \xi_2} \\ \frac{\partial u_w}{\partial \xi_3} \end{Bmatrix}_{jwl} \\
 &= \mathbf{J}_{jwl}^{-1} \begin{Bmatrix} \sum_{o=1}^{N_{\xi_1}} C_{jo}^1(u_w)_{owl} \\ \sum_{o=1}^{N_{\xi_2}} C_{wo}^1(u_w)_{jol} \\ \sum_{o=1}^{N_{\xi_3}} C_{lo}^1(u_w)_{jwo} \end{Bmatrix}_{jwl} = \mathbf{Z}_{jwl} \mathbf{u}_w^e,
 \end{aligned}
 \tag{57}$$

where \mathbf{Z}_{jwl} relates the material gradient of the Cauchy pore pressure at a point to the element pore pressure vector. Introduction of Eqs. (50) and (57) into Eq. (56) and integration over t_n and t_{n+1} by the backward Euler scheme yield

$$\begin{aligned}
 \mathbf{K}_{ct}^e \Delta \mathbf{d}^e - \Delta t \mathbf{K}_L^e \Delta \mathbf{u}_w^e &= \mathbf{R}_p^e, \\
 \mathbf{R}_p^e &= \Delta t \left[\mathbf{R}_q^e + \mathbf{K}_L^e (\mathbf{u}_w^e)^n \right],
 \end{aligned}
 \tag{58}$$

where the coupling matrix \mathbf{K}_{ct}^e , the permeability matrix \mathbf{K}_L^e , and the element load vector resulting from the normal filtration velocity on the boundary \mathbf{R}_q^e are given by

$$\begin{aligned}
 \mathbf{K}_{ct}^e &= \sum_{j=1}^{N_{\xi_1}} \sum_{w=1}^{N_{\xi_2}} \sum_{l=1}^{N_{\xi_3}} \mathbf{W}_j \mathbf{W}_w \mathbf{W}_l |\mathbf{J}|_{jwl} \mathbf{G}_{jwl}^T \mathbf{M}_{jwl}^{n+1T} \mathbf{B}_{jwl}^1, \\
 \mathbf{K}_L^e &= \sum_{j=1}^{N_{\xi_1}} \sum_{w=1}^{N_{\xi_2}} \sum_{l=1}^{N_{\xi_3}} \mathbf{W}_j \mathbf{W}_w \mathbf{W}_l |\mathbf{J}|_{jwl} \mathbf{Z}_{jwl}^T (\mathbf{K}_{w0})_{jwl} \mathbf{Z}_{jwl}, \\
 \mathbf{R}_q^e &= \sum_{j=1}^{N_q} \sum_{w=1}^{N_{j1}} \sum_{l=1}^{N_{j2}} \mathbf{W}_w \mathbf{W}_l |\bar{\mathbf{J}}|_{wl} \mathbf{D}_{wl}^v (V_n)_{wl}^{n+1},
 \end{aligned}
 \tag{59}$$

with \mathbf{D}_{wl}^v being the connectivity matrix for the boundary nodal pore pressure and the element pore

pressure vector, i.e., $\delta(\Delta \mathbf{u}_w)_{wl} = \delta \Delta \mathbf{u}_w^{eT} \mathbf{D}_{wl}^v$. Finally, the following algebraic equations are obtained:

$$\begin{Bmatrix} \mathbf{K}_s^e & \mathbf{K}_c^e \\ \mathbf{K}_{ct}^e & -\Delta t \mathbf{K}_L^e \end{Bmatrix} \begin{Bmatrix} \Delta \mathbf{d}^e \\ \Delta \mathbf{u}_w^e \end{Bmatrix} = \begin{Bmatrix} \mathbf{R}_F^e \\ \mathbf{R}_p^e \end{Bmatrix}.
 \tag{60}$$

After the assemblage of Eq. (60) for every element into the global system, the coupled consolidation behavior of saturated soil can be modeled progressively with the given initial and boundary conditions.

3 Numerical examples

3.1 One-dimensional hyperelastic consolidation

To verify the accuracy of the present formulation, the 1D consolidation problem studied by Borja and Alarcón (1998) will be re-considered. The soil skeleton is assumed to be hyperelastic with a strain energy function defined as

$$\psi = \frac{1}{2} \lambda (\varepsilon_1 + \varepsilon_2 + \varepsilon_3)^2 + \mu (\varepsilon_1^2 + \varepsilon_2^2 + \varepsilon_3^2),
 \tag{61}$$

where λ and μ are the material constants. The soil is loaded suddenly by a uniform pressure with the intensity of $F_0=90$ kPa (Fig. 3). Excess pore pressure is zero at the top and it is impervious at all other boundaries. Vertical displacement of the bottom surface and horizontal displacement of the side surfaces are fixed. The material properties are: the two constants associated with the strain energy function $\lambda=57.7$ kPa, $\mu=38.5$ kPa, the permeability coefficient $k_w=1 \times 10^{-8}$ m², the dynamic viscosity of pore fluid $\mu_w=1 \times 10^4$ Pa·s. To compare with the available data in (Borja *et al.*, 1998), the permeability index is taken as an infinite value. Define the non-dimensional time $T_v = k_w t (\lambda + 2\mu) / (\mu_w H_0^2)$, where H_0 is the initial depth of the soil. The time increment is taken as $\Delta T_v=0.0001$.

The problem is solved by the QEM using one quadrilateral quadrature element and by the commercial software ABAQUS using linear elements CPE4P for verification. The convergence of the pore pressure at the center of the soil column is displayed in Fig. 4 where the convergent ABAQUS results

are used as reference. It is seen that much faster convergence is achieved by the QEM. It should be mentioned that, in the QEM, the order of the element should not be too high (less than 15). Otherwise the efficiency will be decreased. For a given problem, if the required accuracy is not reached, the order of the element should be increased, and more elements will be used if the order of the element attains the preset maximum value.

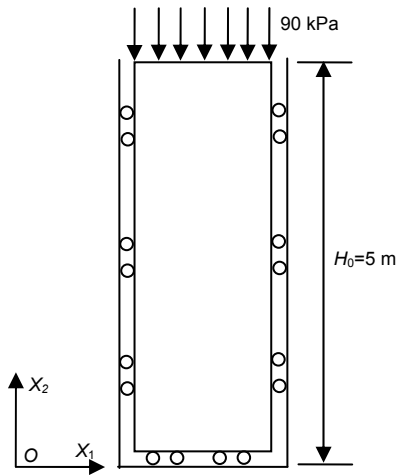


Fig. 3 One-dimensional hyperelastic consolidation

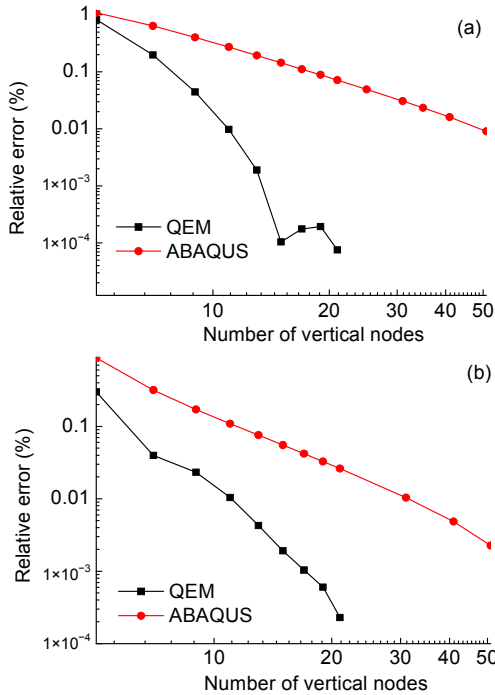


Fig. 4 Convergence of pore pressure in 1D hyperelastic consolidation: (a) $T_v=0.03$; (b) $T_v=0.06$

The obtained total hydraulic head is compared with those in (Borja *et al.*, 1998) and the ABAQUS solution in Fig. 5, where x_2 is the coordinate in the deformed configuration. Thirty linear elements in the FEM and one quadrilateral quadrature element with two integration points in the horizontal direction and 11 integration points in the vertical direction are employed. It is seen that the results of the present formulation agree well with those of ABAQUS, but small deviations are observed between those in (Borja *et al.*, 1998) and the present formulation. The deviation is presumed to result from the inadequate number of pore pressure nodes used in (Borja *et al.*, 1998).

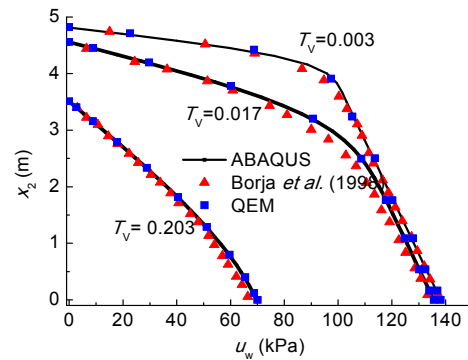


Fig. 5 Cauchy pore pressure in 1D hyperelastic consolidation

The influence of non-Darcian flow is then considered and the corresponding results of pore pressure are given in Fig. 6. It is observed that with the increase of the parameters of the non-Darcian model, the rate of consolidation decreases.

The effect of geometric nonlinearity is studied, and the problem is also solved under the condition of small deformation. The corresponding material constants for small deformation consolidation analysis are: Young's modulus $E_0=100$ kPa, Poisson's ratio $\nu_0=0.3$. The results of the ultimate settlements obtained by the respective small deformation and finite deformation schemes and the relative errors are shown in Fig. 7 where v' is the settlement of large deformation consolidation analysis. It is observed that in small deformation consolidation analysis, the ultimate settlement varies linearly with the external loads; in finite deformation consolidation analysis, however, with the increase of the external loads, the rigidity of the soil skeleton increases, and the

settlement increases rather moderately in comparison with that of the small deformation analysis. The relative error of settlement for small deformation analysis rises with the increase of the load and reaches 100% when the load is equal to the modulus E_0 . Thus, the influence of geometric nonlinearity has to be considered when the settlements are large.

3.2 Two-dimensional hyperelastic consolidation

The 2D consolidation problem shown in Fig. 8 is considered. The strain energy function of the soil skeleton is defined as

$$\psi = \frac{\mu}{2}(\text{tr}(\mathbf{C}) - 3) - \mu \ln J + \frac{\lambda}{2}(\ln J)^2, \quad (62)$$

where λ and μ are the material constants taken as 100 MPa and 30 MPa, respectively. The soil is initially stress-free, and the external load increases linearly to 25 MPa in 2.5 s. For comparison with ABAQUS, Darcy’s law is assumed, and an infinite permeability index is taken. The permeability coefficient is

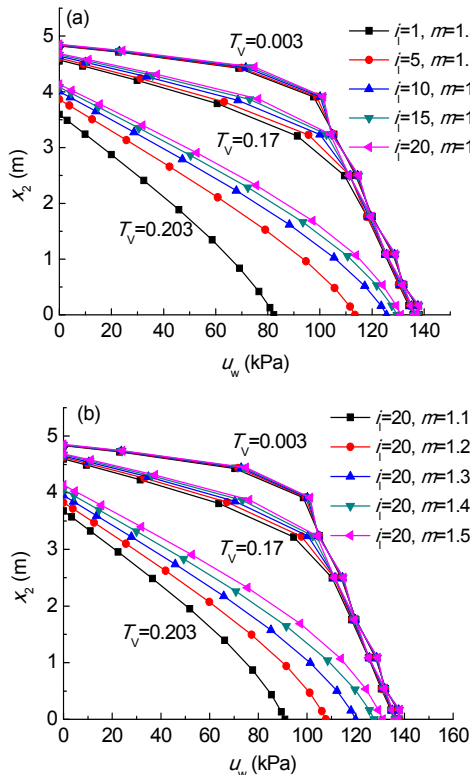


Fig. 6 Effect of non-Darcian flow on hyperelastic consolidation: (a) variation of i ; (b) variation of m

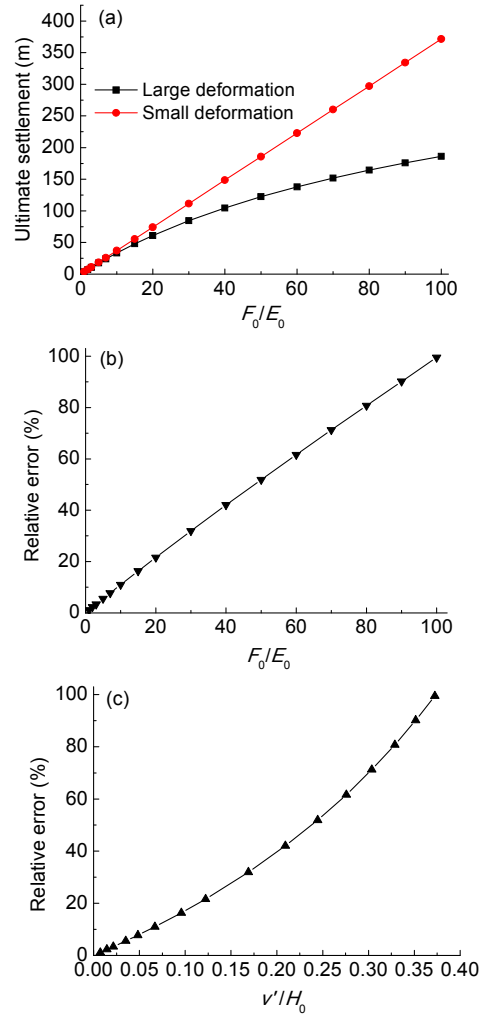


Fig. 7 Effect of geometric nonlinearity on the settlement: (a) variation of the settlement with F_0/E_0 ; (b) variation of the relative error with F_0/E_0 ; (c) variation of the relative error with the relative settlement

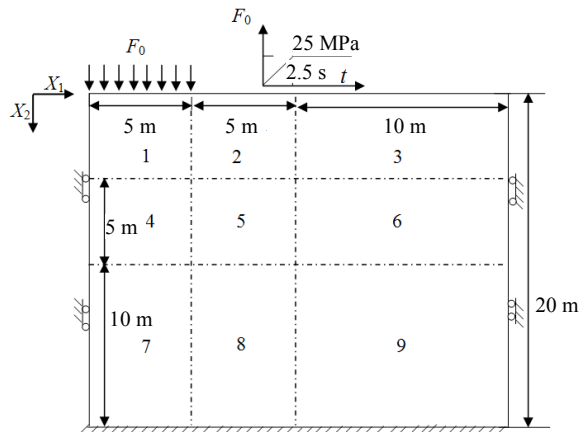


Fig. 8 Two-dimensional consolidation

0.0001 m² and the dynamic viscosity is 1×10⁴ Pa·s. All displacements of the bottom surface and horizontal displacement of the side surfaces are fixed. Nine quadrilateral quadrature elements with 9×9 integration points in each element are used and all the domains of the nine elements are further divided uniformly in ABAQUS, each consisting of 20×20 linear pore pressure elements. The employed time increment is 0.1 s.

The results of the displacement at $X_1=0$ and $X_1=5$ m and the pore pressure along the left edge of the soil are given in Figs. 9 and 10 and compared with those of ABAQUS. Excellent agreement is obtained for all results. The convergence of the Cauchy pore pressure at $X_1=0$, $X_2=2.5$ m is studied and the results of the QEM and ABAQUS are listed in Table 1. A much faster convergence is seen for the QEM: the number of degrees of freedom for the QEM to converge is 1/40 and 1/20 of those by ABAQUS at $t=2.5$ s and $t=5$ s, respectively.

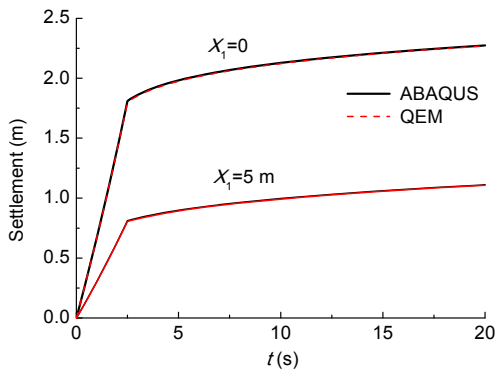


Fig. 9 Settlement of 2D hyperelastic consolidation

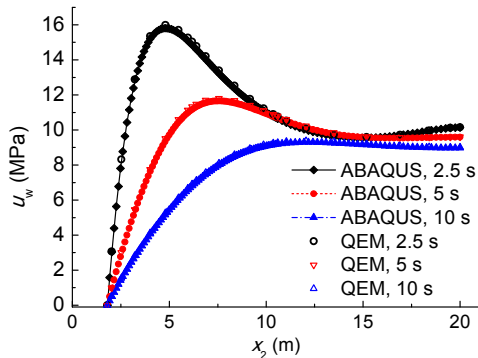


Fig. 10 Pore pressure of 2D hyperelastic consolidation

Table 1 Convergence of Cauchy pore pressure

Degree of freedom	u_w	u_w	u_w	u_w
	(×10 ⁷ Pa) ($t=2.5$ s, QEM)	(×10 ⁷ Pa) ($t=2.5$ s, ABAQUS)	(×10 ⁶ Pa) ($t=5$ s, QEM)	(×10 ⁶ Pa) ($t=5$ s, ABAQUS)
147	1.358	1.688	7.442	7.273
507	1.544	1.564	7.757	7.545
1083	1.536	1.540	7.757	7.607
1875	1.536	1.531	7.756	7.626
2883	1.536	1.527	7.756	7.635
4107	1.536	1.525	7.756	7.640
5547	1.536	1.524	7.756	7.643
23232	–	1.521	–	7.649
41772	–	1.520	–	7.650
65712	–	1.520	–	7.650

3.3 Drained triaxial test

The drained triaxial test given by Al-Tabbaa (1987) and Callari *et al.* (1998) is simulated to verify the formulation of finite deformation elasto-plastic consolidation analysis. The material constants are

$$\tilde{k} = 0.013, \quad \alpha = 90, \quad \tilde{\lambda} = 0.013, \quad M = \begin{cases} 0.8, \\ 0.9. \end{cases} \quad (63)$$

The normally consolidated soil with an initial pressure of 300 kPa is loaded by a deviatoric stress $q=120$ kPa, and then unloaded to 0. An infinite permeability is taken to simulate the totally drained condition. The simulated stress paths are shown in Fig. 11, where p' is the mean Cauchy stress, $\varepsilon_q = \sqrt{2/3} \|e\|$ is the deviatoric strain, and e is the principal logarithmic distortion. Fairly good agreement is reached among the results of the QEM, the experiment, and the literature (Al-Tabbaa,1987; Callari *et al.*, 1998).

3.4 Two-dimensional elasto-plastic consolidation

The geometric properties and boundary conditions of this problem are the same as those in Section 3.2. The material constants for the soil skeleton are the same as those in Section 3.3 and $M=0.9$. The permeability coefficient k_{w0} is equal to 1×10^{-7} m² and the dynamic viscosity is 1×10^4 Pa·s. The permeability index is 0.45 and the initial void ratio is 1.0.

At the beginning, the soil is normally consolidated with a pressure 300 kPa. The load is applied instantly with the magnitude of 300 kPa. 5×5 integration points are used in every element and the time increment is 0.1 d.

The settlement at the left side of the load is given in Fig. 12. It is observed that with the increase of the parameters of the non-Darcian model, the rate of consolidation decreases. Thus, nonlinearity in the flow law will slow down the consolidation process. It is noteworthy that this observation is similar to the conclusion drawn for elastic and small deformation case in (Teh

and Nie, 2002). The distribution of the settlement at $t=100$ d is shown in Fig. 13 and the differential settlement is given in Fig. 14, where $\Delta v'$ is the difference of settlement at $X_1=0$ and $X_2=5$ m, and Δx_1 is the deformed horizontal distance of the two points. Clearly, with the increase of the parameters of the non-Darcian model the differential settlement decreases.

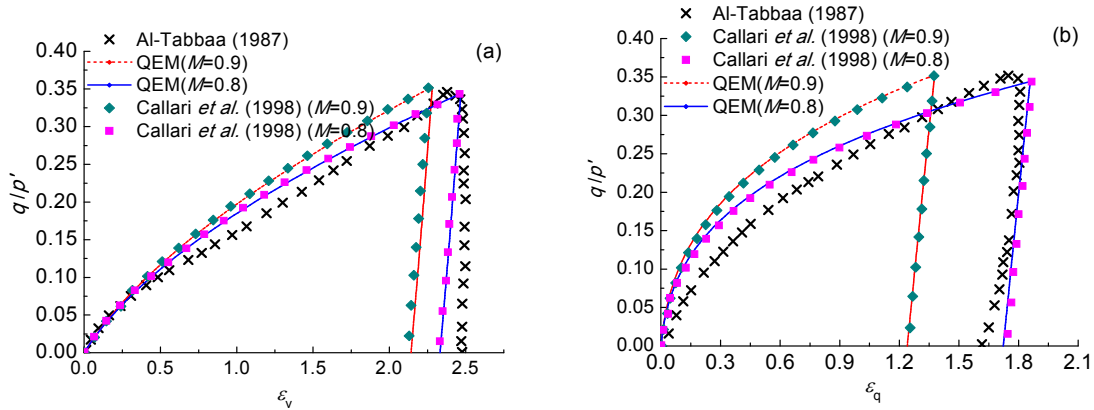


Fig. 11 Simulation of drained triaxial test: (a) ratio q/p' vs. volumetric strain; (b) ratio q/p' vs. deviatoric strain

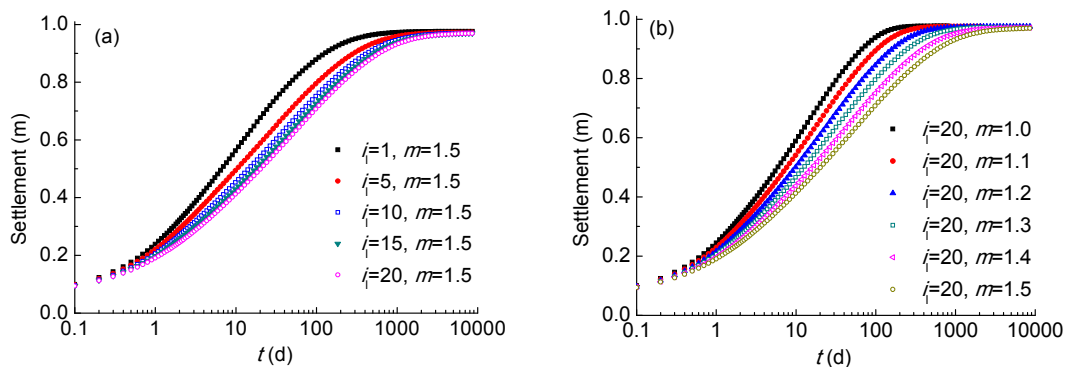


Fig. 12 Effect of non-Darcian flow on elasto-plastic consolidation: (a) variation of i_i ; (b) variation of m

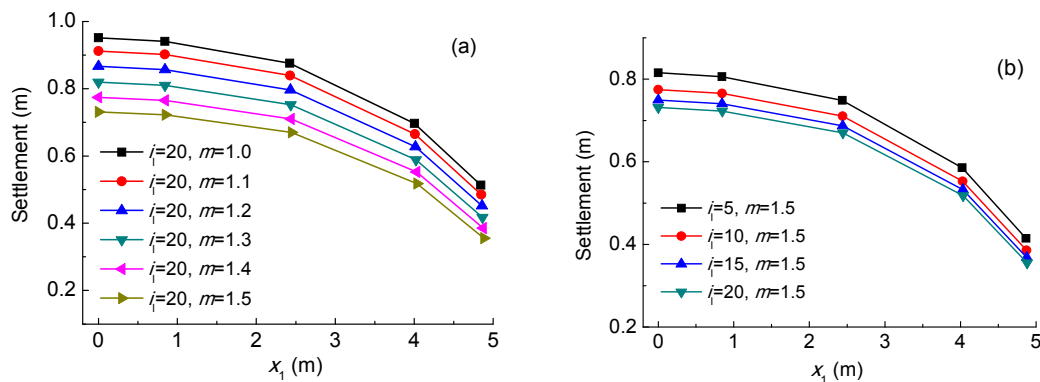


Fig. 13 Effect of non-Darcian flow on distribution of the settlement of elasto-plastic consolidation: (a) variation of m ; (b) variation of i_i

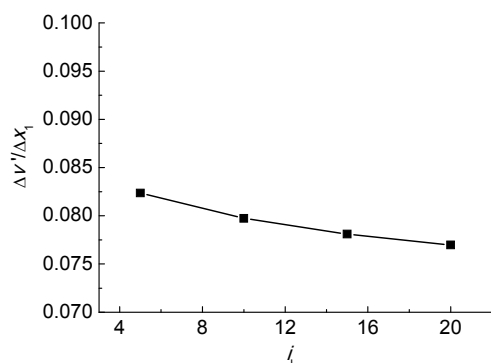


Fig. 14 Effect of non-Darcian flow on the differential settlement of elasto-plastic consolidation

4 Conclusions

The weak form quadrature element method has been applied to finite deformation consolidation analysis in the present work. The weak form description of Biot's model based on the initial configuration has been established and the TL scheme has been employed. The results of the present formulation are compared with those in previous and ABAQUS, and the accuracy of results is validated. The effect of geometric nonlinearity and the non-Darcian flow on consolidation is studied. The following conclusions can be drawn:

1. A much faster convergence is achieved by the QEM than with the FEM, reducing the number of degrees of freedom significantly.
2. In small deformation consolidation analysis, the ultimate settlement varies linearly with the external loads; in finite deformation consolidation analysis, however, the settlement increases rather moderately due to the stiffening of the soil skeleton.
3. With the increase of the non-Darcian model parameters, the rate of consolidation and the differential settlement decrease.

References

- Al-Tabbaa, A., 1987. Permeability and Stress-strain Response of Speswhite Kaolin. PhD Thesis, University of Cambridge, Cambridge, UK.
- Armero, F., 1999. Formulation and finite element implementation of a multiplicative model of coupled poro-plasticity at finite strains under fully saturated conditions. *Computer Methods in Applied Mechanics and Engineering*, **171**(3):205-241. [http://dx.doi.org/10.1016/S0045-7825\(98\)00211-4](http://dx.doi.org/10.1016/S0045-7825(98)00211-4)
- Biot, M.A., 1941. General theory of three-dimensional consolidation. *Journal of Applied Physics*, **12**(2):155-164. <http://dx.doi.org/10.1063/1.1712886>
- Borja, R.I., Alarcón, E., 1995. A mathematical framework for finite strain elastoplastic consolidation. Part 1: balance laws, variational formulation, and linearization. *Computer Methods in Applied Mechanics and Engineering*, **122**(1):145-171. [http://dx.doi.org/10.1016/0045-7825\(94\)00720-8](http://dx.doi.org/10.1016/0045-7825(94)00720-8)
- Borja, R.I., Tamagnini, C., Alarcón, E., 1998. Elastoplastic consolidation at finite strain part 2: finite element implementation and numerical examples. *Computer Methods in Applied Mechanics and Engineering*, **159**(1): 103-122. [http://dx.doi.org/10.1016/S0045-7825\(98\)80105-9](http://dx.doi.org/10.1016/S0045-7825(98)80105-9)
- Callari, C., Auricchio, F., Sacco, E., 1998. A finite-strain Cam-clay model in the framework of multiplicative elasto-plasticity. *International Journal of Plasticity*, **14**(12):1155-1187. [http://dx.doi.org/10.1016/S0749-6419\(98\)00050-3](http://dx.doi.org/10.1016/S0749-6419(98)00050-3)
- Carter, J.P., Small, J., Booker, J.R., 1977. A theory of finite elastic consolidation. *International Journal of Solids and Structures*, **13**(5):467-478. [http://dx.doi.org/10.1016/0020-7683\(77\)90041-5](http://dx.doi.org/10.1016/0020-7683(77)90041-5)
- Carter, J.P., Booker, J.R., Small, J.C., 1979. The analysis of finite elasto-plastic consolidation. *International Journal for Numerical and Analytical Methods in Geomechanics*, **3**(2):107-129. <http://dx.doi.org/10.1002/nag.1610030202>
- Gibson, R., England, G., Hussey, M., 1967. The theory of one-dimensional consolidation of saturated clays. *Geotechnique*, **17**(3):261-273. <http://dx.doi.org/10.1680/geot.1967.17.3.261>
- Hansbo, S., 1997. Aspects of vertical drain design: Darcian or non-Darcian flow. *Geotechnique*, **47**(5):983-992. <http://dx.doi.org/10.1680/geot.1997.47.5.983>
- Hansbo, S., 2001. Consolidation equation valid for both Darcian and non-Darcian flow. *Geotechnique*, **51**(1):51-54. <http://dx.doi.org/10.1680/geot.2001.51.1.51>
- He, R., Zhong, H., 2012. Large deflection elasto-plastic analysis of frames using the weak-form quadrature element method. *Finite Elements in Analysis and Design*, **50**: 125-133. <http://dx.doi.org/10.1016/j.finel.2011.09.003>
- Kuang, L.W., 2010. Finite Element Analysis of Large Deformation Consolidation of Soft Clays Based on Biot's Theory. MS Thesis, Jinan University, Guangzhou, China (in Chinese).
- Lewis, R.W., Roberts, G.K., Zienkiewicz, O.C., 1976. A non-linear flow and deformation analysis of consolidation problems. *Numerical Methods in Geomechanics*, **2**: 1106-1118.
- Li, T., 2001. Large Deformation Consolidation Theory Based on the U.L. Description and the Finite Element Analysis. MS Thesis, Chang'an University, Xi'an, China (in Chinese).

- Miehe, C., 1996. Numerical computation of algorithmic (consistent) tangent moduli in large-strain computational inelasticity. *Computer Methods in Applied Mechanics and Engineering*, **134**(3):223-240.
[http://dx.doi.org/10.1016/0045-7825\(96\)01019-5](http://dx.doi.org/10.1016/0045-7825(96)01019-5)
- Mikasa, M., 1965. The consolidation of soft clay. *Civil Engineering in Japan*, **1**(1):21-26.
- Mo, Y., Ou, L., Zhong, H., 2009. Vibration analysis of Timoshenko beams on a nonlinear elastic foundation. *Tsinghua Science & Technology*, **14**(3):322-326.
[http://dx.doi.org/10.1016/S1007-0214\(09\)70047-1](http://dx.doi.org/10.1016/S1007-0214(09)70047-1)
- Preisig, M., Prévost, J.H., 2011. Stabilization procedures in coupled poromechanics problems: a critical assessment. *International Journal for Numerical & Analytical Methods in Geomechanics*, **35**(11):1207-1225.
<http://dx.doi.org/10.1002/nag.951>
- Prévost, J.H., 1983. Implicit-explicit schemes for nonlinear consolidation. *Computer Methods in Applied Mechanics and Engineering*, **39**(2):225-239.
[http://dx.doi.org/10.1016/0045-7825\(83\)90022-1](http://dx.doi.org/10.1016/0045-7825(83)90022-1)
- Sandhu, R.S., Wilson, E.L., 1969. Finite element analysis of seepage in elastic media. *Journal of the Engineering Mechanics Division, ASCE*, **95**(3):641-652.
- Simo, J., 1992. Algorithms for static and dynamic multiplicative plasticity that preserve the classical return mapping schemes of the infinitesimal theory. *Computer Methods in Applied Mechanics and Engineering*, **99**(1):61-112.
[http://dx.doi.org/10.1016/0045-7825\(92\)90123-2](http://dx.doi.org/10.1016/0045-7825(92)90123-2)
- Simo, J., Meschke, G., 1993. A new class of algorithms for classical plasticity extended to finite strains. Application to geomaterials. *Computational Mechanics*, **11**(4):253-278.
<http://dx.doi.org/10.1007/BF00371865>
- Slepicka, F., 1960. Contribution to the solution of the filtration law. International Union of Geodesy and Geophysics, Commission of Subterranean Waters, p.245-258.
- Teh, C.I., Nie, X.Y., 2002. Coupled consolidation theory with non-Darcian flow. *Computers and Geotechnics*, **29**(3):169-209.
[http://dx.doi.org/10.1016/S0266-352X\(01\)00022-2](http://dx.doi.org/10.1016/S0266-352X(01)00022-2)
- Wang, D., Xie, P., Lu, H., 2013. Meshfree consolidation analysis of saturated porous media with stabilized conforming nodal integration formulation. *Interaction & Multiscale Mechanics*, **6**(2):107-125.
<http://dx.doi.org/10.12989/imm.2013.6.2.107>
- Xie, Y.L., Pan, Q.Y., Zeng, G.X., 1994. Three-dimensional finite deformation consolidation theory based on the spatial description. *Journal of Chang'an University (Natural Science Edition)*, **4**:6-12 (in Chinese).
- Xie, Y.L., Pan, Q.Y., Zeng, G.X., 1995. Three-dimensional finite deformation consolidation theory based on the material description and the finite element solution. *Journal of Zhejiang University (Natural Science Edition)*, **4**:476-485 (in Chinese).
- Yuan, S., 2015. Analysis of Saturated and Unsaturated Soils by the Weak Form Quadrature Element Method. PhD Thesis, Tsinghua University, Beijing, China (in Chinese).
- Yuan, S., Zhong, H., 2014. Consolidation analysis of non-homogeneous soil by the weak form quadrature element method. *Computers and Geotechnics*, **62**:1-10.
<http://dx.doi.org/10.1016/j.compgeo.2014.06.012>
- Yuan, S., Zhong, H., 2015. Weak form quadrature element analysis of seepage problems. *Journal of Geotechnical Engineering*, **37**(2):257-262 (in Chinese).
- Zhong, H., Gao, M., 2010. Quadrature element analysis of planar frameworks. *Archive of Applied Mechanics*, **80**(12):1391-1405.
<http://dx.doi.org/10.1007/s00419-009-0388-9>
- Zhong, H., Wang, Y., 2010. Weak form quadrature element analysis of Bickford beams. *European Journal of Mechanics-A/Solids*, **29**(5):851-858.
<http://dx.doi.org/10.1016/j.euromechsol.2010.03.012>

中文概要

题目: 软粘土弹塑性大变形的求积元法分析

目的: 考虑几何非线性及非达西渗流对软粘土固结的影响, 提出一种大变形固结问题的求积元求解列式, 以提高数值方法的计算精度及计算效率。通过数值算例研究几何非线性及非线性渗流定律对软粘土固结的影响, 为工程实际提供参考。

创新点: 1. 提出一种大变形固结问题的高阶数值求解方法; 2. 在固结问题求解中同时考虑几何非线性及非线性渗流定律。

方法: 1. 基于初始构型, 采用完全拉格朗日格式, 建立大变形固结问题求解列式; 2. 基于变形梯度乘法分解, 得到大变形条件下的土体本构模型; 3. 基于指数关系的渗流定律, 建立渗流连续性方程; 4. 通过数值算例验证方法, 研究几何非线性及非达西渗流对软粘土固结的影响。

结论: 1. 所建立的求积元方法的收敛速度要远远快于有限元法, 降低了问题计算规模; 2. 在小变形条件下, 最终沉降随外荷载线性变化, 而在大变形条件下, 随着载荷的增大, 沉降相对于小变形条件有所降低; 3. 当考虑非达西渗流定律时, 软粘土的固结速率随着非达西渗流参数的增加而降低。

关键词: 弱形式求积元法; 大变形弹塑性固结; 软粘土; 变形梯度乘法分解; 非达西定律; 比奥固结